THE PENNSYLVANIA STATE UNIVERSITY
SCHREYER HONORS COLLEGE

DEPARTMENT OF ELECTRICAL ENGINEERING

Millimeter-Wave Radar Imaging of an Automobile

ABIGAIL ELIZABETH WAGNER
SPRING 2022

A thesis
submitted in partial fulfillment
of the requirements
for a baccalaureate degree
in Electrical Engineering
with honors in Electrical Engineering

Reviewed and approved* by the following:

Mahanth Gowda
Assistant Professor of Computer Science and Engineering
Thesis Supervisor

Timothy Kane
Professor of Electrical Engineering
Honors Adviser

* Electronic approvals are on file.

ABSTRACT

Autonomous vehicles need robust sensing capabilities to make safe driving decisions, but most modern obstacle detection approaches rely on light-based systems (i.e., cameras and lidar), which can be unreliable in challenging weather and lighting conditions. This research applies millimeter-wave (mmWave) radar to image an automobile. Phase and signal strength are recorded at points in a grid layout facing the vehicle using a frequency-modulated continuous wave radar (FMCW) operating at 77 GHz. All data is collected using electromagnetic simulation software. Each set of simulated measurements is converted to a heatmap for observation. The resulting images include some visual indicators of a car's presence but will require future signal processing work or higher resolution simulations for practical use.

TABLE OF CONTENTS

LIST OF FIGURES

LIST OF TABLES

ACKNOWLEDGEMENTS

I would like to extend my sincere appreciation to everyone who made this research possible. Thank you to Dr. Mahanth Gowda, my thesis supervisor, for challenging me with the opportunity to explore this interesting project and for providing the technical guidance to complete it. Many thanks to my honors adviser, Dr. Timothy Kane, for invaluable advice throughout the thesis process and over the past four years that has changed how I think about being an (electrical) engineer. I would also like to thank Bailey Campbell for sharing her HFSS expertise and helping me build useful simulations. Finally, I am grateful to all of my mentors, friends, and family, for their inspiration and support during my time at Penn State.

Chapter 1

Introduction

Automotive traffic accidents are a leading cause of death worldwide with approximately 1.3 million fatalities each year [1]. An additional 20 to 50 million people suffer non-fatal injuries, many of whom experience long-term disability. By automating environment perception, decision-making, and vehicle response [2], autonomous vehicles (AVs) have the potential to significantly reduce accidents by addressing the root cause of 94% of crashes: human error [3]. Already, lower levels of automation such as basic forward-collision warning and automatic braking have corresponded to a 7% and 14-15% reduction in crashes, respectively [4]. Recent estimates project that fully autonomous vehicles could account for up to 15% of passenger vehicles sold worldwide in 2030, contributing to an overall 30% growth in the automotive industry that will generate up to $1.5 trillion in additional revenue [5]. However, analysts caution that in a low-disruption scenario, technical and regulatory delays could slow consumer uptake and limit this scale of AV adoption until 2040 or beyond. A series of high-profile accidents during AV testing [6][7] have shaken public confidence in the technology, so demonstrating reliable driving performance is a necessity not only for improving traffic safety, but also for achieving a widespread rollout to maximize the technology's positive impact.

Automakers' autonomous driving capabilities currently vary. Based on the five Levels of Driving Automation defined by the Society of Automotive Engineers (SAE) [8], as shown in Figure 1, major AV competitors like Argo [9], Cruise [10], and Waymo [11] remain stalled at level 4. Level 4 vehicles are capable of fully automated driving under almost all conditions but

may be unsuited for challenging scenarios like darkness, weather events (rain, snow, fog), and unmarked rural roads [8][11]. Commercially available technologies such as Tesla's Autopilot feature are only at level 2 and are still classified as driver support features, not automated driving features [11].

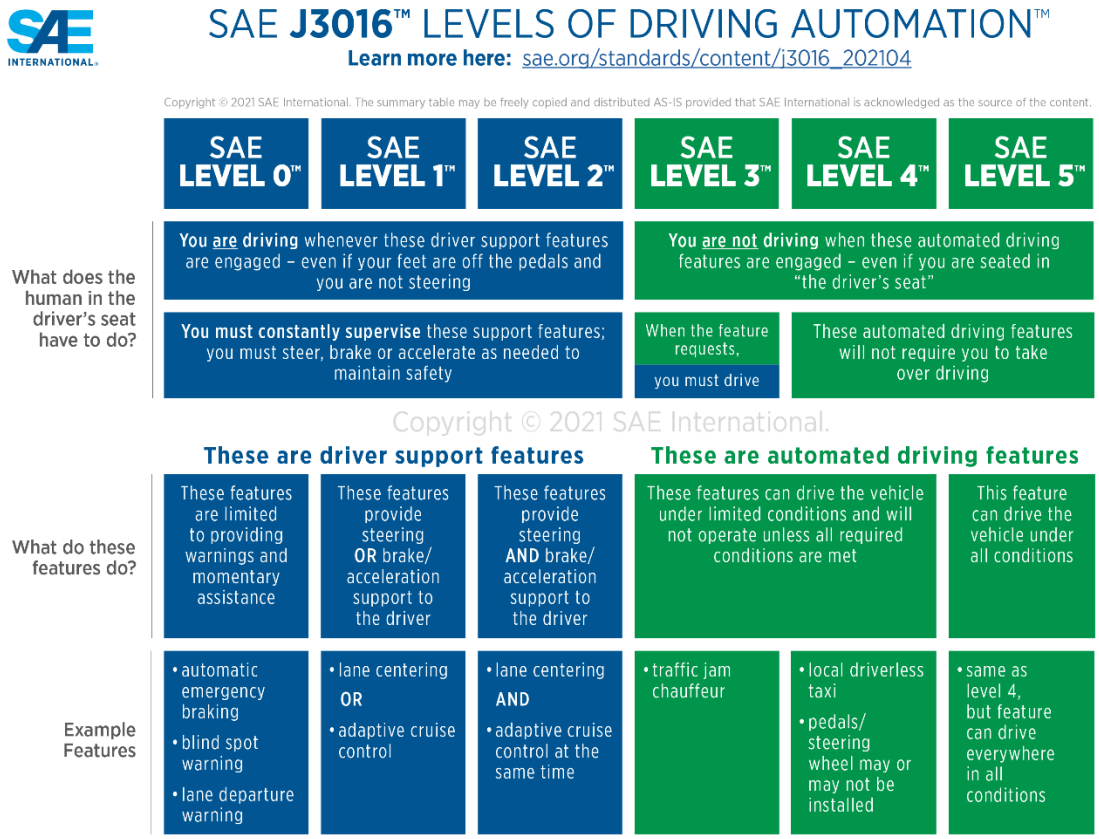

Figure 1. Society of Automotive Engineers (SAE) Levels of Driving Automation. From [8].

Autonomous vehicles must be capable of accurately detecting obstacles to reliably make safe driving decisions, so their sensing systems are one of their most important components. Four types of sensing have been considered: ultrasound, radar, lidar, and optical cameras. The first three use active illumination with sound, microwaves, and light, respectively, while cameras

passively collect reflected light [12]. Their benefits and drawbacks are summarized in Table 1. Most AVs currently use lidar or cameras combined with post-processing algorithms to interpret their surroundings [13]. Because both approaches rely on reflected light (lidar, short for "light detection and ranging," captures reflections from actively emitted laser beams, and cameras receive ambient light, sometimes with the aid of illumination), they are unreliable in challenging lighting and weather conditions such as fog and dust [13][14]. Precipitation also poses a challenge for light-based systems, both while it falls and when it collects on sensors to block their view [11]. When sensing systems fail, the vehicle cannot accurately detect obstacles or continue driving safely. Developing sensing systems that are robust under adverse weather conditions is necessary to achieve level 5 autonomy.

Table 1. Benefits and Drawbacks of Sensor Technologies. Adapted from [12].

Technology	Benefits	Drawbacks
Ultrasonic	Low cost Small package	Limited range (5 m) No angular measurement No range resolution Affected by dirt and wind
Radar	Moderate cost Range up to 200 m Good distance and velocity accuracy Fair resolution Insensitive to dust, fog, and lighting	Sparse point clouds due to specular reflections Limited azimuth resolution
Lidar	High range accuracy High resolution High azimuth resolution and wide field of view (FOV) Dense point clouds due to scattering from metallic and non-metallic objects	High cost Limited range Velocity is calculated, not measured Sensitive to dust and inclement weather
Camera	Moderate cost High azimuth accuracy and wide FOV Strong target classification under ideal conditions	Limited range Less accurate range detection Less robust velocity estimation Affected by dirt, lighting, and visual obstruction

Millimeter wave (mmWave) radar, operating at frequencies in the 30 – 300 GHz range [15], offers a potential alternative to light-based sensing systems. The longer wavelengths it transmits and collects are less susceptible to lighting challenges and certain weather types than lidar is. Radar and lidar perform comparably in the presence of precipitation; based on atmospheric measurements, as shown in Figure 2, electromagnetic waves in the frequency ranges for mmWaves and visible light experience similar attenuation levels in rain. Large raindrops and snow present challenges for both sensor types by collecting on lenses and antennas, and as they fall, they can scatter both radar and lidar beams.

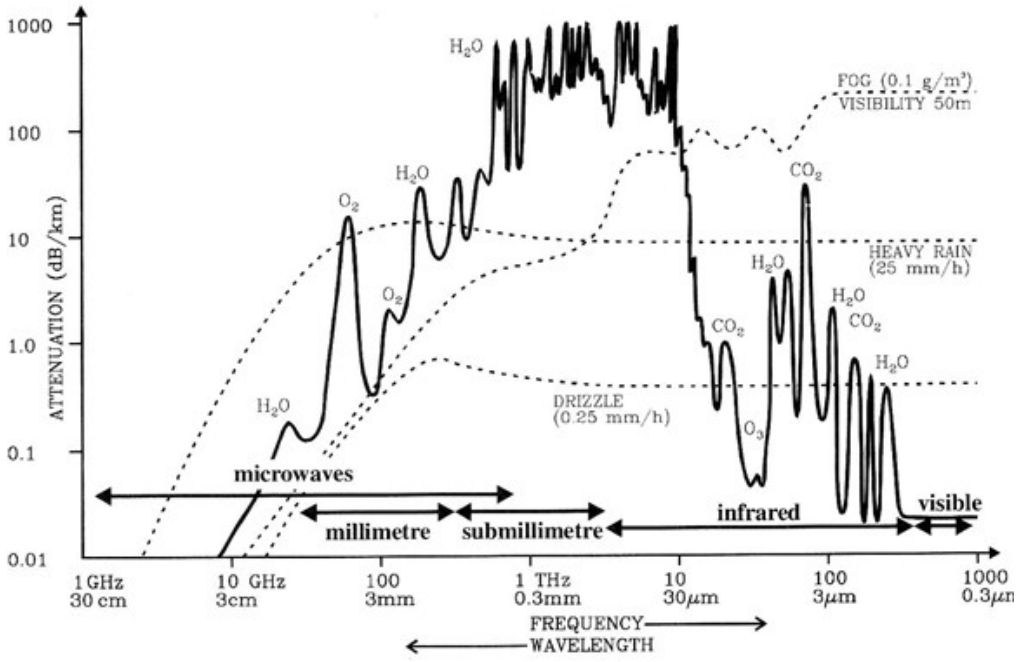

Figure 2. Atmospheric attenuation for a nominal clear atmosphere, with additional attenuation shown for fog and rain. From [16].

For other types of weather, such as dust, dirt, fog, and aerosols, radar operates reliably despite experiencing some attenuation losses, and it is unaffected by darkness. It can be mounted behind painted plastic covers for easier integration on a vehicle, boasts farther range detection

than lidar (up to 200 m), and has a lower cost to implement [12]. However, automotive radar usage today is typically limited to location and speed detection [14]. Unlike with lidar, the waves used by radar experience specular reflections, which scatter in different directions and do not always return to the receiver antenna(s) [13]. As a result, the data points available for post-processing are sparser than with lidar and make object identification challenging. Additionally, radar systems experience noise from sensor leakage, background clutter, and multipath effects that can lead to false detections. If the impact of specular reflections and noise can be mitigated, then mmWave radar could provide a reliable sensing supplement or alternative under conditions where light-based systems are insufficient.

Challenges of Using mmWave Radar for Imaging

One of the main challenges when working with mmWave radar for automotive applications is the specular reflections it experiences. Specular reflection describes the phenomenon when a wave cleanly reflects off a surface such that the angle of incidence equals the angle of reflection [17]. This type of reflection occurs when the irregularities of the reflecting surface are small compared to the wavelength of the incident wave, such as when light reflects off a mirror. Because most of a car's surface is smooth compared to mmWave wavelengths, automotive radar experiences specular reflections. As future automotive radar systems push toward the upper boundaries of the mmWave band, specular reflections will become less pronounced of an issue, but as long as most usage is around 77 GHz, they remain a concern. In contrast, the wavelengths of light used by lidar are small relative to a car's surface irregularities, and the light scatters in multiple directions from the target [13]. Since mmWaves reflect

specularly, they only return to the receiver when the radar beam is approximately normal to the specular surface [14]. When the radar beam is not normal to the target, most waves bounce off the car without returning to the receiver, resulting in a sparser point cloud than could be found with lidar. Point clouds for outdoor scenarios are inherently sparse because of the volume of open space between objects, so the sparsity from specular reflections exacerbates the problem. The sparsity of data from these lost reflections is independent of the radar's resolution, so upgrading the hardware alone will not fix the problem [13]. Even if a rotating radar is used to capture a large physical aperture, specular objects constrain the useful field of view to a smaller effective aperture [14]. As a result, radar signal processing for target detection and identification becomes more challenging.

In addition to specular reflections, radar is susceptible to clutter and noise. In an automotive scenario, especially in urban settings, other objects will be present. Reflectors like roads and buildings can cause ghost objects, which occur when additional reflections of an original object are detected due to multipath. Other objects that pose no driving risks, such as swarms of insects, can also reflect mmWaves and cause false alarms [13]. Additionally, mmWaves interact differently with different types of materials, so point clouds for automotive scenarios are often non-uniform. Because of the combined effects of specular reflections and noise from scene diversity, creative solutions are needed to achieve reliable target detection and identification using radar.

Approaches to Implementing a mmWave Radar for Vehicle Identification

Existing research has taken a variety of approaches to mitigate these challenges. In [13], researchers found that with only two optimally spaced radars, they could use deep learning to build and train a network capable of real-time lidar- or camera-like perception. By formulating radar spacing as an optimization problem, they found that once the distance between two radars was comparable to or slightly greater than a vehicle's width, the average error rate for angle estimation dropped significantly. The performance continued to improve slightly for distances greater than a vehicle's width, but the most dramatic increase occurred around the width of a car. Radar spacing is also constrained by the size of the vehicle on which the sensors are to be mounted, so while spacing distances greater than the vehicle's width could improve performance, they are unrealistic to implement. For all separation distances tested, the setup with two radars always had a lower average error rate than a single radar. Introducing multiple radars creates a larger virtual aperture, increasing both the number of reflections captured (resulting in a denser point cloud) and the probability of capturing part of an object that may be occluded in another view (resulting in a more complete point cloud). Therefore, including more than one radar can reduce the impact of specular reflections to improve data collection, and spacing radars at about the same width as the target object can improve system accuracy while meeting vehicle mounting constraints.

Instead of using more than one radar to increase the effective aperture, another team of researchers [14] drew inspiration from synthetic aperture radar (SAR) by taking advantage of a car's motion to capture different points. SAR uses a moving radar and multiplexes the collected measurements over time to artificially create a larger aperture. Requirements for SAR include exact knowledge of the platform's trajectory and velocity as well as access to a powerful

processor to synthesize the stored data and account for Doppler effects [18]. By coherently combining radar measurements as the car moves and accounting for the delays between multiple pairs of transmitter (Tx) and receiver (Rx) antennas to estimate the radar's location (a necessary step for applying standard SAR processing techniques), they achieved sharper images than with a non-coherent approach. The team then generated a 3D point cloud from their measurements using a novel multi-focusing algorithm, but no new processing techniques for the resulting cloud are explored. Additionally, their system cannot currently process radar data in real time.

An SAR-based approach was criticized in [13] for not providing enough variety of viewpoints to combat specular reflection. Concern was also raised that motion-based SAR is only useful for side-looking sensors because they are the only parts of the car whose aperture will increase with forward vehicle motion. Although side-looking sensors could have useful applications for parking spot detection, they would not contribute to forward-looking obstacle detection. A forward-looking SAR was implemented in [19] with strong results but used a beam scanning 300 GHz radar, a frequency significantly higher than typical automotive radar frequencies, which reside around 77 GHz.

Additionally, motion-based SAR lacks the height information needed to generate a 3D point cloud. Because the aperture moves in only one dimension, the SAR projects a 3D scene onto a 2D plane, and information about the vertical dimension is lost. The authors of [2] note that any mmWave radar (not just SAR) consisting of only a horizontal antenna array faces the same lack of information about scene height. Research in [14] uses a radar with multiple vertical Tx/Rx antenna pairs to estimate the heights of scatter points and fuses that data with the 2D image. This approach can discriminate objects at different heights but is unable to image vertically. To achieve vertical imaging, either a vertical antenna array of comparable dimension

to the target object or a smaller array with digital beamforming to sweep across different elevation angles is needed. However, such a vertical array would be too large to mount on a vehicle, and the beam scanning approach would require too many measurements to achieve reasonable angular resolution (i.e., 1°), making it unrealistic for autonomous driving at typical speeds.

In addition to addressing specular reflections, researchers are concerned with mitigating the effects of noise. Researchers in [13] developed a pre-processing method to reduce noise before feeding point clouds to their deep learning network. Because their system used more than one radar, they could compare the space coherence between both measurements to eliminate noise, based on the observation that non-noise points were more likely to appear in the point clouds of multiple radars. Simple averaging would have been insufficient for removing noise because the different radars capture points in different places. Similarly, the team analyzed time coherence between sequential measurements to estimate a moving vehicle's pose.

After preparing the data, the team in [13] chose to use deep learning to process these point clouds and set up a bounding box around each detected object. A deep learning approach is appealing because it could learn from the non-uniform point cloud distributions and better adapt to the wide range of possible orientations than if specific features or filters were crafted for all cases by hand. However, such an approach requires a large amount of data for training and validation. The computational demands for any type of machine learning are significant, and they are especially high for deep learning because such an algorithm must implement multiple layers of artificial neural networks [20]. Because research into mmWave radar for vehicle identification is relatively new and data is not widely available, the team needed to generate their own dataset for training and validation. Ultimately, their network delivered lidar- or camera-like

perception that they expect could be improved further with access to a higher resolution radar to produce a denser point cloud.

To avoid the drawbacks of deep learning, other systems may use more standard radar signal processing techniques that are less data-hungry and less computationally demanding. For example, many systems apply a chain of fast Fourier transforms (FFTs) to the received signal to resolve and estimate quantities like the range, velocity, and angle of an object [20]. Additional processing techniques available include a constant false alarm rate (CFAR) algorithm, which helps detect targets in the presence of background noise by measuring noise in the vicinity, and density-based spatial clustering of applications with noise (DBSCAN), which forms clusters of points within a specified distance from each other to better differentiate multiple targets in a scene. Researchers in [19] achieved promising results for a forward scanning SAR automotive radar using back-projection algorithms coupled with compressed sensing techniques to reconstruct SAR scans. The details of these algorithms are outside the scope of this thesis, but more information can be found in the original references.

When conducting experiments, teams in [13] and [14] tested their systems on vehicles with real hardware. Researchers in [19] used simulations and a more controlled lab setting with small-scale vehicles and clutter, while [2] worked virtually in MATLAB to evaluate simple simulation scenarios by reducing cars and trucks to box shapes.

Chapter 2

Materials and Methods

This thesis seeks to image a stationary vehicle using mmWave radar and achieve a high enough resolution that the vehicle is visually recognizable. Experiments are conducted in two stages.

The first stage, preliminary simulations, addresses subcomponents of the overall scenario, including the radar's antenna pattern and the radar cross-section (RCS) of a vehicle. Antenna parameters such as dimensions and operating frequency are modeled after a commercially available automotive radar. The RCS is generated using a generic 3D automobile model. These components were initially modeled and computed with the intention of reducing the computational demands of later ray tracing simulations for more complex scenarios.

The second stage of experiments simulates a composite automotive radar scenario incorporating a vehicle, a radar, and a road. Radar samples are taken in a grid pattern slightly wider and taller than the target vehicle, in line with recommendations from other researchers' findings. Phase and signal strength measurements are collected to form composite intensity images. Data collection is completed using electromagnetic simulation software but uses detailed models true to real vehicle shape and incorporates information about material properties.

Preliminary Simulations

The initial steps of the experimental setup included modeling an automotive radar's antenna pattern and computing the RCS for a generic automobile using electromagnetic simulation software. The motivation behind simulating measurements of these two components

was to use the results in later ray tracing simulations for large-scale automotive scenario analysis. By precomputing the antenna pattern and the vehicle's RCS, the computational demand of these large-scale simulations could be reduced.

All simulations at this stage were performed using Feko and WinProp, two high-frequency computational electromagnetics software packages distributed by Altair. Feko is well-suited for scenarios which require precise analysis of electromagnetic wave interactions, such as antenna design, electromagnetic interference, and computation of radar cross-sections [21]. It includes multiple frequency-domain solution methods and one in the time-domain, as well as hybridization options to maximize efficiency for a particular application. WinProp focuses instead on wave propagation analysis and is appropriate for larger-scale problems with less required precision, such as antenna coverage and wireless network planning [22]. Feko was used to calculate the antenna pattern and vehicle RCS, while WinProp was used to run a ray tracing simulation with a radar and the vehicle RCS.

The radar model upon which the simulations are based is the AWR1843AOP frequency-modulated continuous wave (FMCW) radar, sold by Texas Instruments and marketed for automotive applications [23]. A patch antenna model was created in Feko to conform to the specifications of one of the three transmitter antennas on the radar. This model is shown in Figure 3. The model settings included a 1.3 V power supply and a source frequency ranging from 76 to 81 GHz, as indicated in the radar's datasheet. The dimensions of the square patch were not given in the datasheet but were roughly estimated to be 1.53 mm by 1.53 mm. The material composition information also was not provided, so generic parameters were chosen based on examples in the Feko documentation [21]. These parameters included modeling the metal patch

as a perfect electrical conductor and the substrate as a lossless dielectric with $\varepsilon_r = 2.2$ and a depth of 2.87 mm.

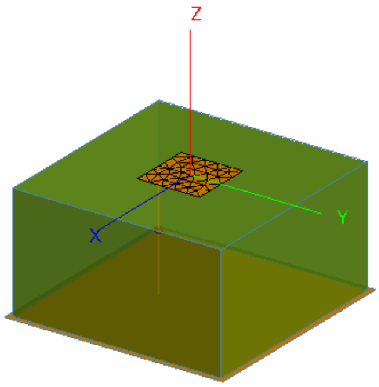

Figure 3. Patch Antenna Model

Running a simulation with this one Tx antenna in the radar's propagation frequency range provided graphs of its far-field gain measurements, which are shown in Figure 4. In the far-field plot, theta represents the elevation angle in degrees (°). The radar datasheet provides plots of the average effective isotropic radiated power (EIRP) for each transmitter antenna across changes in the elevation angle. Feko does not provide the option to plot EIRP, but it is possible to compare the Feko plots of antenna gain with respect to theta to those of EIRP with respect to theta. Since EIRP can be represented as

$$EIRP = output\ power - cable\ loss\ (dB) + antenna\ gain\ (dBi) \quad (1)$$

and cable loss is assumed to be negligible to simplify this experiment, the Feko far-field gain plot is expected to have the same shape as the datasheet's EIRP plot, except that the gain plot will be shifted lower along the vertical axis. Comparing the far-field plot in Figure 4 with a sample plot from the datasheet in Figure 5, it is observed that the shapes of the graphs align well, that both appear to roll off in magnitude at around 80°, and that the gain graph is indeed shifted

downward relative to the EIRP graph. Therefore, although specific numerical quantities were not verified, the general design of the modeled antenna is likely appropriate to simulate the radar transmitters. This single antenna setup and simulation was initially designed as a stepping stone to a model of the full radar, which includes three Tx antennas, four Rx antennas, and coordinated behavior among them. However, a detailed radar model was not needed for the later ray tracing simulations, so the results of this model were not used in later experiments.

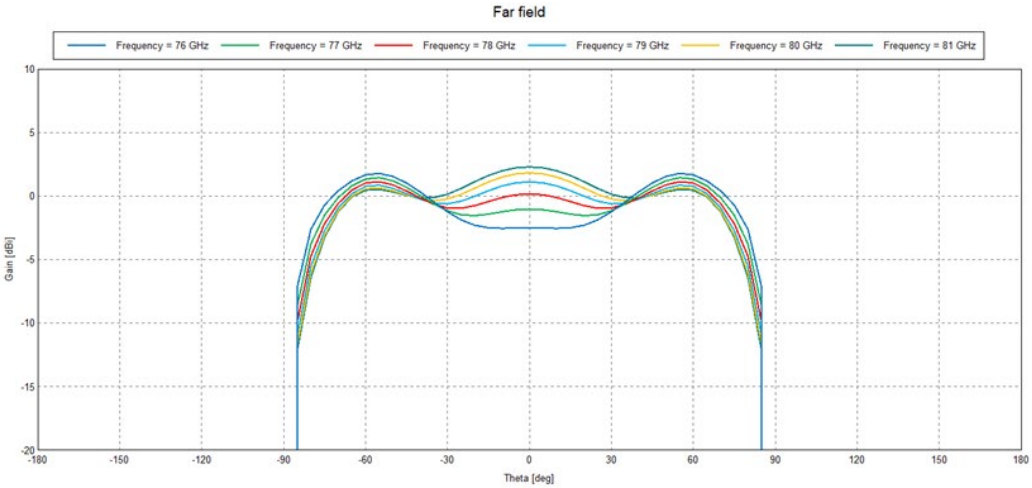

Figure 4. Far-Field Gain Measurements from Patch Antenna Simulation

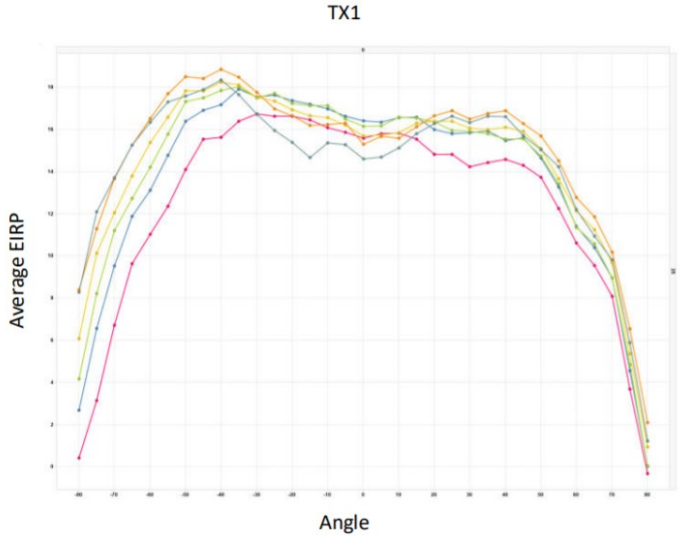

Figure 5. Plot of Average EIRP vs. Elevation Angle for Tx1 on Automotive Radar. From [23].

After modeling a simple antenna, the next step was to model a target vehicle. To run wave propagation scenarios in WinProp to measure the radar response, it is useful to have a simplified model of the target object to reduce computational demands. Therefore, Feko was used to generate the RCS of the vehicle so it could later be used as the target object in WinProp. After initially attempting to import a detailed 3D car model, it became clear the available computational resources could not support the model's complexity. Instead, a simple, generic model of the back of a car provided in the Feko Component Library was used.

From this model, an RCS was generated in Feko using a plane wave source with linear polarization that was designed to capture reflections from a range of incident angles, as shown in Figure 6. The magnitude of the plane wave was set at 1.3 V based on the radar datasheet. Due to limited computational resources, the highest source frequency that resulted in a successful simulation was 1 GHz when the model was meshed at the coarse setting. Unfortunately, this frequency is nearly two orders of magnitude below the operating frequency of the automotive radar. Although the simulation does not precisely imitate the radar transmitter, the computed RCS provides a coarse version of what the radar is capable of measuring.

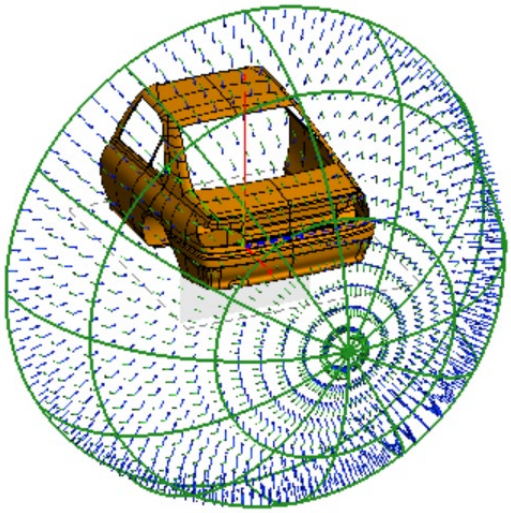

Figure 6. Plane Wave Source for RCS Computation

The simulated RCS can be plotted for a fixed azimuth (theta') or elevation (phi') angle against a sweep of the non-fixed angle (note that these variables have changed from their definitions in the previous section because of an axis rotation during the simulation, as indicated by the prime notation (')). The point at the base of the back of the vehicle is defined as theta' = 0°, phi' = 0°. Figure 7 plots a horizontal sweep of the RCS in dB around the base of the model (i.e., RCS vs. theta' with fixed phi' = 0°). Figure 8 plots a vertical sweep of the RCS in dB around the sides of the model at 45° and 90° from the center of the back (i.e., RCS vs. phi' with fixed theta' = 45° or 90°).

The shape of Figure 7 seems reasonable, as the local peaks in RCS at -90°, 0°, and 90° align with the expectation that more of the incident wave will be reflected back when theta' causes the wave to be nearly perpendicular to the large surfaces on the sides and back of the vehicle. In Figure 8, it is notable that the RCS for a fixed theta' is nearly a mirror image of the RCS when theta' is fixed at the negative of that angle. This observation aligns with the near symmetry of the car model across the yz-plane.

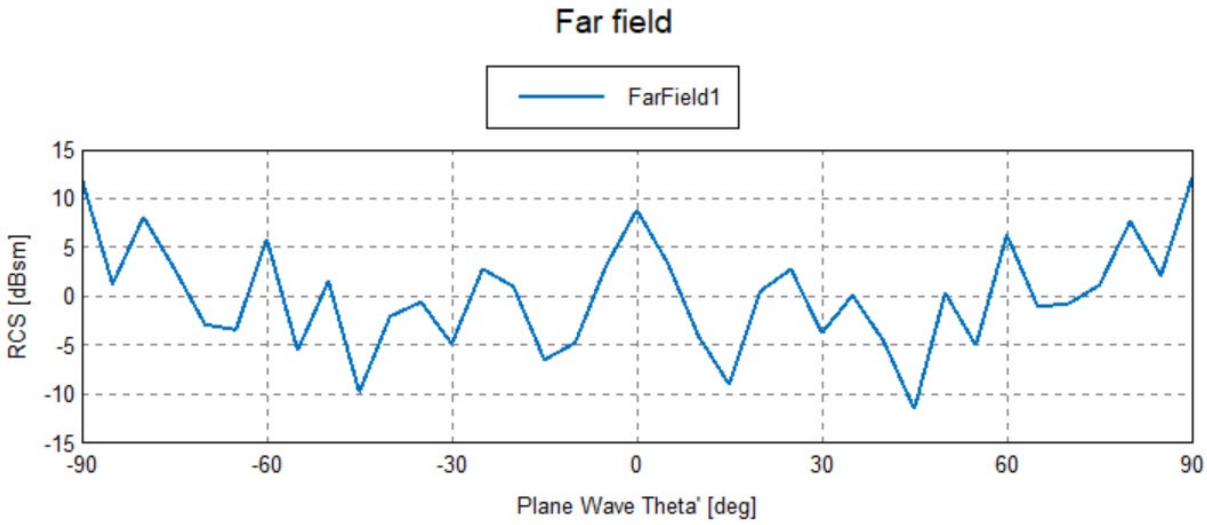

Figure 7. Plot of RCS Against the Azimuth Angle when the Elevation Angle is Fixed at 0°

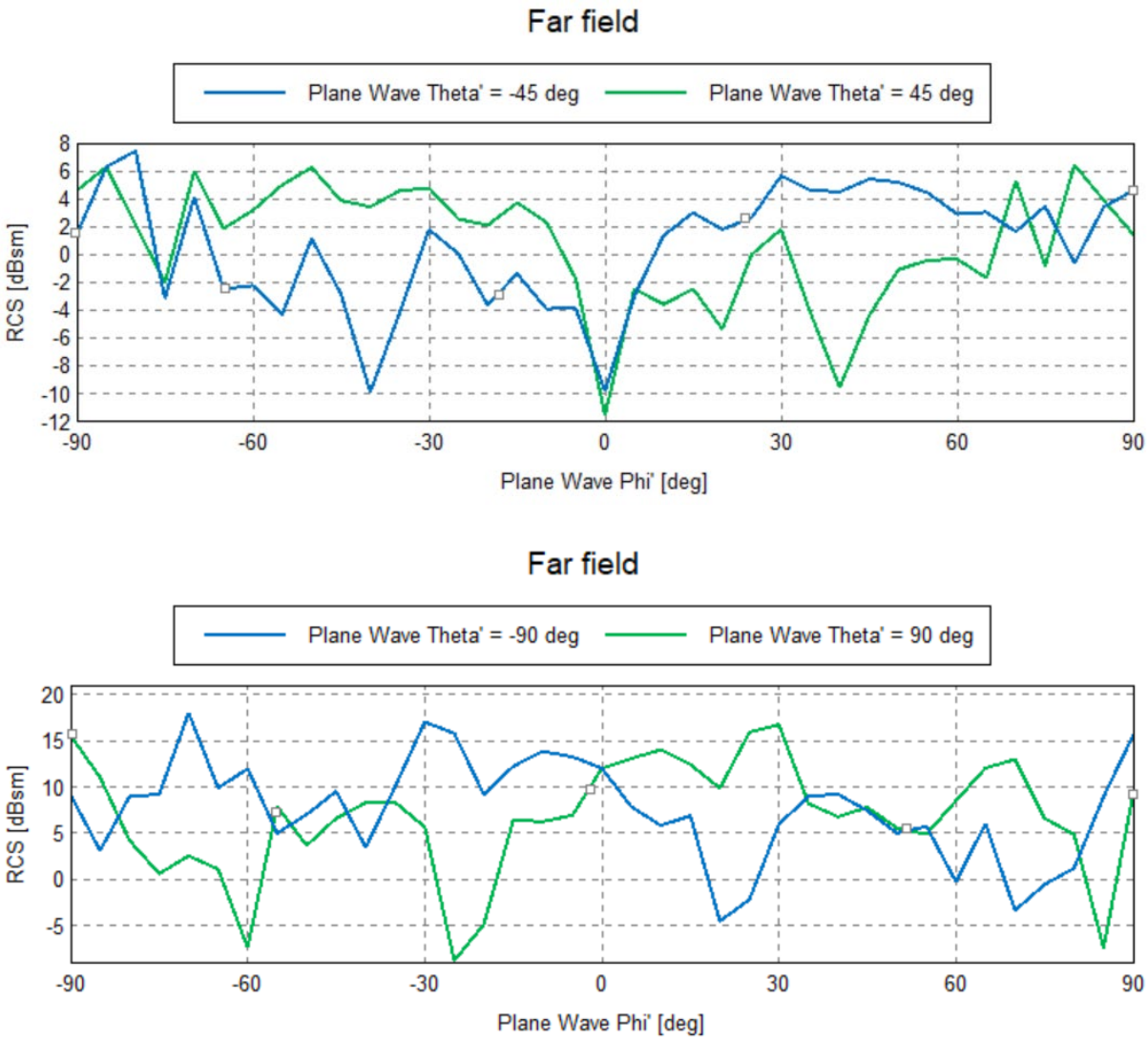

Figure 8. Plot of RCS Against the Elevation Angle when the Azimuth Angle is Fixed at (top) 45° and (bottom) 90°

Once the RCS was generated, it could be imported into WinProp for efficient standard ray tracing simulation of the scenario. However, attempts to run a ray tracing simulation using the RCS were unsuccessful because of difficulties using the software to properly overlay the RCS on a simple box object, as is the recommended approach in the documentation. The decision was made to instead perform scenario-level ray tracing simulations with a different

software package, as discussed in the next section. Although the RCS information generated in Feko was not eventually used at the scenario level, it demonstrated an approach to generating an RCS for a vehicle that could be used if the computational needs of future experiments demand a simplified model.

Automotive Radar Scenario

After considering two important subcomponents of an automotive radar scenario, a set of simulations featuring electromagnetic interactions between a vehicle, road, and radar were conducted. Due to software challenges in Feko and WinProp with computing the vehicle RCS at the desired frequencies for automotive radar and using it in ray tracing simulations, all measurements for this stage were conducted using simulations in Ansys HFSS SBR+. HFSS SBR+ is a solver that uses shooting and bouncing rays (SBR) to model electromagnetic interactions in electrically large environments [24]. It is an asymptotic, high-frequency structure simulator (HFSS) and is suitable for the mmWave frequencies used in automotive radar. The basic Ansys HFSS software (without SBR+) is a 3D electromagnetic field simulator for designing high-frequency electronics, including antennas and arrays, radio frequency (RF) and microwave components, and more [25]. The HFSS SBR+ solver uses SBR to simulate near-field and far-field radiation patterns, antenna performance, and radar signatures in electrically large environments with reduced computational time and resources compared to a full-wave solver like the basic HFSS. However, HFSS SBR+ uniquely overlays advanced diffraction physics including physical theory of diffraction (PTD), uniform theory of diffraction (UTD), and creeping wave (CW) physics to improve SBR accuracy, and it keeps analysis times short using

software features like multicore central processing unit (CPU) use and graphic processing unit (GPU) acceleration.

In these experiments, two different scenarios were tested: a car on a road and an empty road. Including a road allows for a more realistic scenario than if the simulations were conducted in free space, and testing both scenarios provides opportunities for direct comparison. Additionally, the radar was moved to different positions around the car (front, side, and front corner) to test different viewpoints. Figure 9 depicts a sample front-facing simulation setup.

The radar is made to face the car at a distance of about 10 m from the car's surface. Distances are measured from the center of the car body, so to achieve a distance of about 10 m from the outside of the body, the front-facing position places the radar 12 m from center, the side-facing position places the radar 11 m from center, and the corner-facing position places the radar 12 m from center. The 10 m distance was chosen to provide sufficient stopping distance for a car moving at 25 mph, a typical speed limit for urban environments. The following stopping distance calculation was used [26]:

$$d = \frac{{v_o}^2}{2\mu g} \tag{2}$$

In this formula for stopping distance, v_o is the vehicle speed in m/s, μ is the coefficient of kinetic friction, and g is standard acceleration due to gravity. A speed of 25 mph is equivalent to $v_o =$ 11.176 m/s, and a typical coefficient of friction for a vehicle with normally driven and worn tires is $\mu = 0.7$. The result of the calculation is a stopping distance $d \approx 9$ m. Higher-speed scenarios or drivers with tires in poor condition will need a longer stopping distance, but for a simple urban traffic scenario, 10 m is a reasonable distance at which to test the radar.

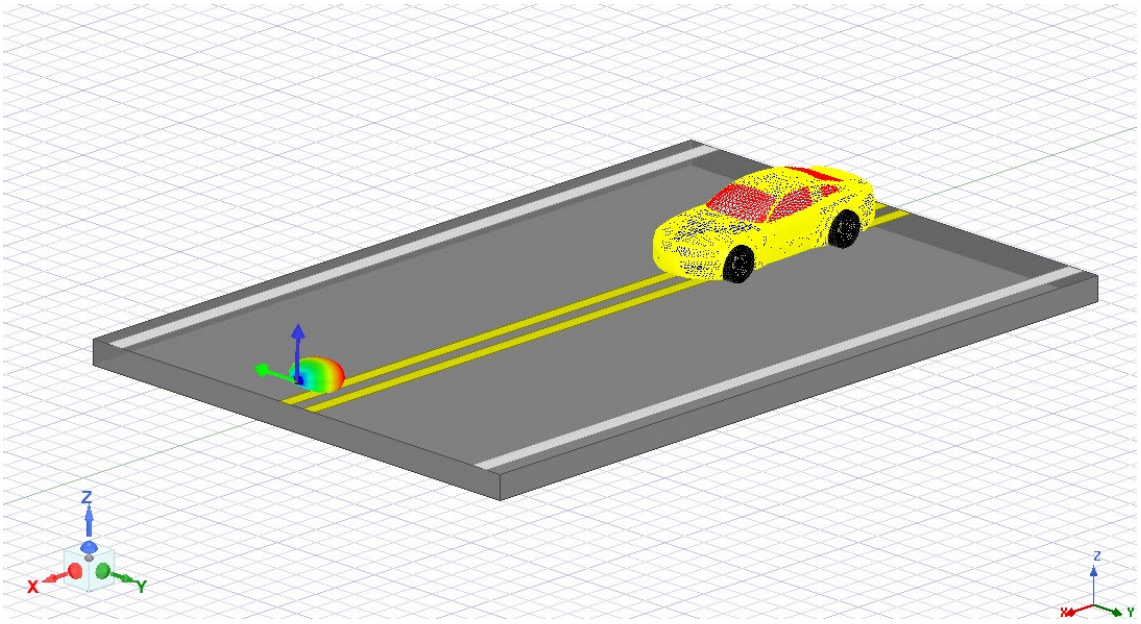

Figure 9. Simulation Setup for Vehicle on Road, Measured from Front

Models with realistic size, shape, and material compositions were used in the simulation. The target car was a Ford Mustang Coupe for which the windows were modeled as glass ($\varepsilon_r = 5.5$), the body and wheels as perfect electrical conductors ($\sigma \to \infty$), and the interior as a vacuum ($\varepsilon_r = 1$). In the simulation, the car body and wheels were modeled as $\sigma =$ 1e+30 S/m to approximate $\sigma \to \infty$ for a perfect conductor, but choosing a σ on the order of 10^7 would be sufficient to represent steel ($\sigma =$ 1.01e+7 S/m) or aluminum ($\sigma =$ 3.69e+7 S/m) [27]. The road was straight and flat with lane marker lines, and it was given the properties of asphalt ($\varepsilon_r = 6.25$). Both models were developed by Ansys and are available in the example project "Autonomous Vehicular Radar_ADP" included in Ansys Electronic Desktop 2021. Dimensions for these model objects are given in Table 2. HFSS SBR+ is capable of running ray tracing scenarios with a 3D model directly, so the intermediate RCS generation step originally conducted in Feko as part of the preliminary simulations was no longer necessary.

The radar used in the simulations is a FMCW radar with one Tx antenna and one Rx antenna, which are roughly co-located. It transmits at a center frequency of 77 GHz, typical for automotive radar. Additional parameters and simulation settings are listed in Table 3. To reduce simulation time, the maximum number of bounces is limited to 3.

Radar measurements of the scene are taken by moving the radar to 100 different points spaced evenly in a square 6 m grid facing the target vehicle. For the front- and side-facing measurements, the grid is centered on the car to capture its full dimensions and improve the chances of catching reflections that may be lost from certain angles. The grid spacing differs slightly for the corner-facing position, which collects 100 different points using angle parameters to sweep the radar from 0° to 60° in the azimuth direction (with 0° being normal to the front of the vehicle) and 0° to 10° in the elevation direction (with 0° being at road level). The primary quantities of interest are the phase (in °) and signal strength (in dB) of the received signal. Phase is of interest because it contains a rich set of information about scene depth and reflected wave arrival time for FMCW radars, while signal strength offers a more direct picture of the reflected waves as linked to scene depth and reflector materials. These two quantities are exported from the simulation at the center frequency (77 GHz) as a CSV file for further processing.

Each CSV file is manually reformatted to create a 10 x 10 matrix of measurements corresponding to the grid layout in the simulation. The reformatted file is then loaded into a MATLAB script to generate a heatmap for each scenario showing the relative intensity values. The scope of this thesis is limited to a visual analysis of these images, but future work could explore image processing techniques, possibly including deep learning-based classifiers.

Table 2. Model Dimensions

Vehicle Dimensions (Coupe Mustang)	
Max Length	4.750 m
Max Width	1.825 m
Max Height	1.352 m
Road Dimensions	
Length	15.425 m
Width	10.5 m
Thickness	0.5 m

Table 3. Radar and Waveform Parameters

Radar Configuration	
Setup	Range-Doppler
Waveform Type	Chirp-Sequence FMCW
Channel Configuration	I-Channel
Center Frequency	77 GHz
A/D Sampling Rate	20 MHz
Range Resolution	0.1 m
Range Period	20 m
Velocity Resolution	1 m/s
Velocity Min	-10 m/s
Velocity Max	50 m/s
Horizontal Beam Width	60 deg
Vertical Beam Width	30 deg
Antenna Polarization	Composite
Waveform Parameters	
Bandwidth	1.5 GHz
Chirp Duration	20 us
Frequency Ramp Rate	75 MHz / µs
# A/D Samples per Chirp	400
Pulse (Chirp) Repetition Frequency	30.8 kHz
Chirp Duty Cycle	61.6%

Chapter 3

Results and Discussion

The heatmaps generated from the phase and signal strength measurements for different scenarios were visually evaluated for their imaging effectiveness. Criteria for the images to be considered effective were the presence of a shape resembling the outline of a car, or of distinguishing vehicle features such as wheels or a windshield. Figures 10, 11, and 12 depict these heatmaps for a radar facing the front, side, and front corner of the car, respectively. Each figure includes heatmaps with the car on the road, an empty road, and the difference between these two measurements.

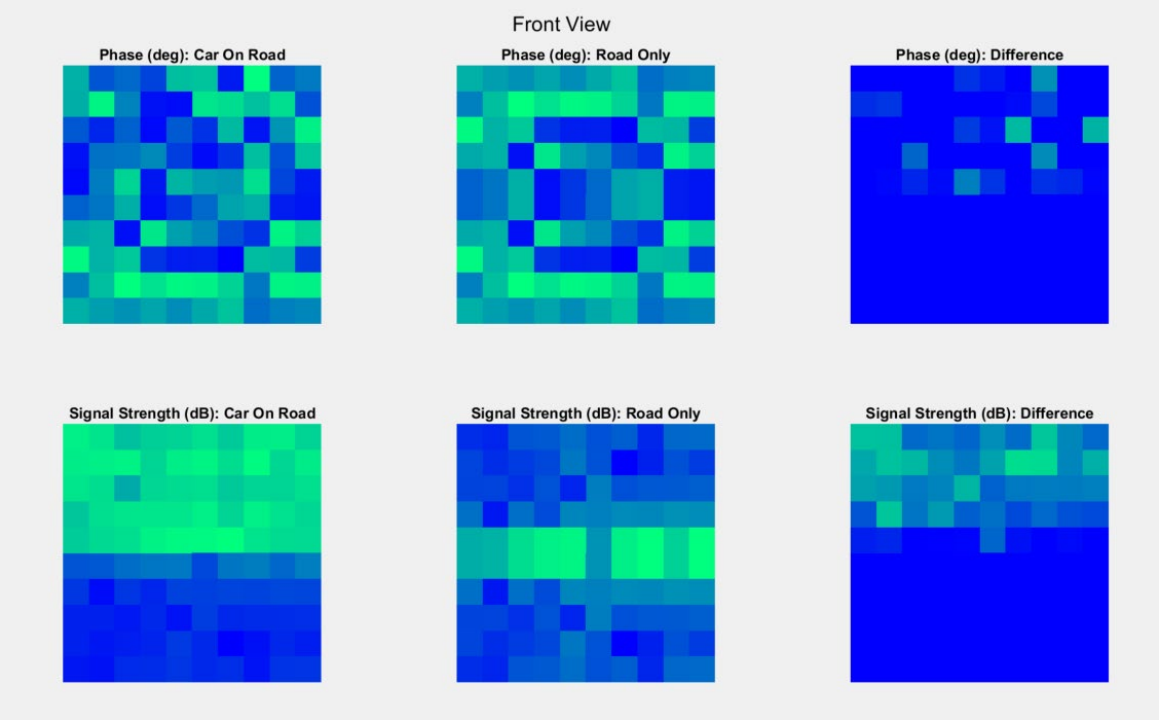

Figure 10. Front View of Car, Measurements in Different Scenarios (dark blue = low value, bright green = high value)

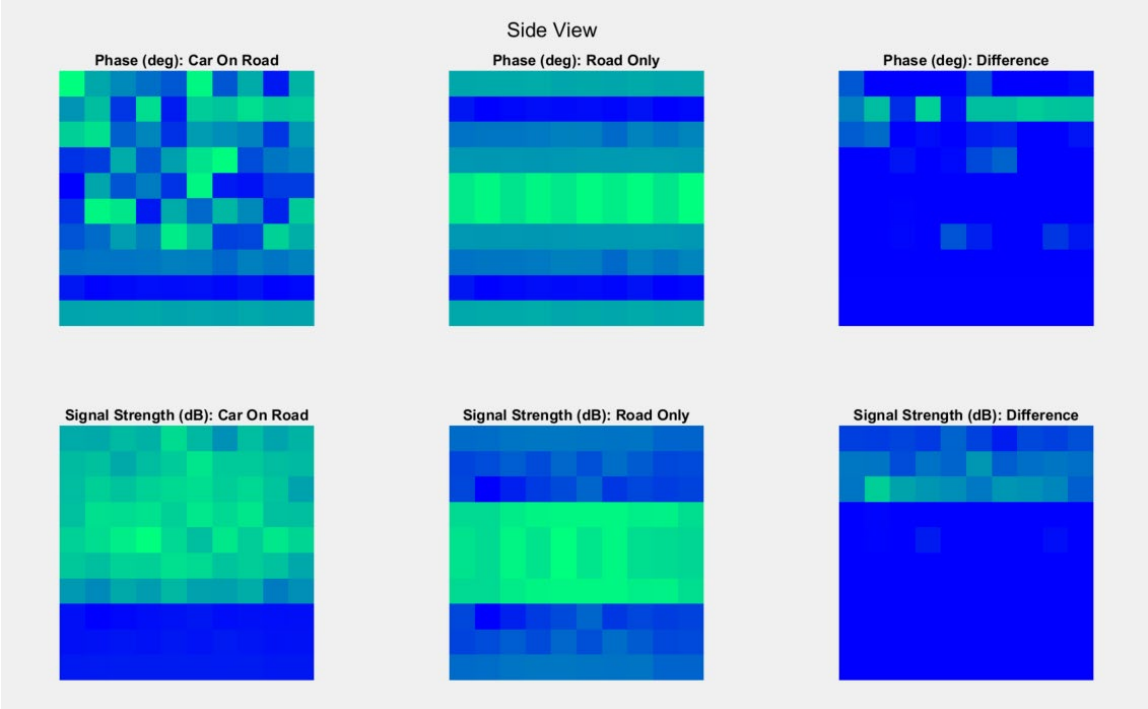

Figure 11. Side View of Car, Measurements in Different Scenarios (dark blue = low value, bright green = high value)

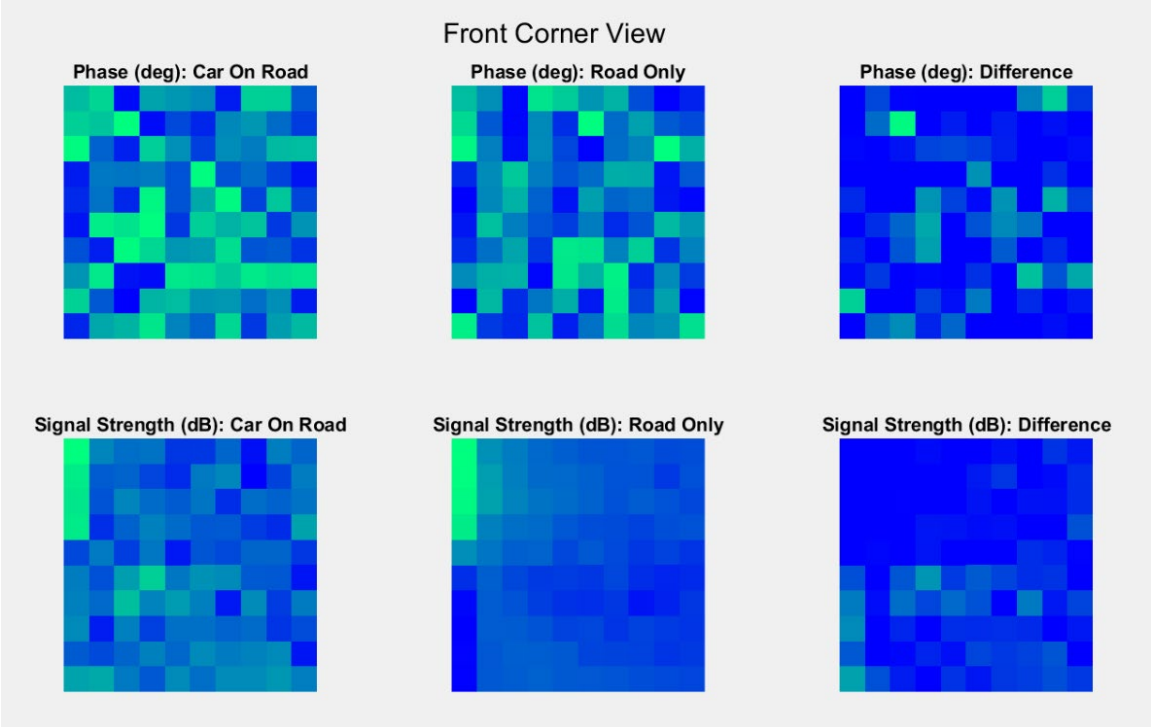

Figure 12. Corner (Front) View of Car, Measurements in Different Scenarios (dark blue = low value, bright green = high value)

Observing the images, phase initially appears to be nonuniform and does not seem to be a useful quantity for direct visual analysis. However, because FMCW radars rely heavily on phase information for extracting data, it is possible these measurements contain useful information that could be uncovered with the right image processing techniques. Since there is no obvious pattern within the phase images, a deep learning approach may be preferred over hand-crafted filters to find meaning in the phase data. Because of the large amount of data and computational resources required, it would likely be best to begin with traditional radar signal processing approaches such as FFT chains, CFAR algorithms, and potentially DBSCAN algorithms before investing in deep learning.

The signal strength heatmaps also do not depict a clear outline of a car or obvious vehicle features, but they do provide some useful cues. Because the simulation setup for the front- and side-facing views centered a square sample grid on the vehicle, approximately the top half of each image corresponds to the region above the road's surface. Compared to the empty road scenario, the car on the road experienced a stronger signal response in this upper region for both the front and side views. The pixels toward the center of these images also appear brighter than the edges, which aligns with the expectation that as the car body curves at the edges, specular reflections become more common. Altogether, this approach to radar data collection was not successful at imaging the car, as defined by producing a visually recognizable outline or identifiable vehicle features. There is, however, a visible difference in signal strength between the car and no car scenarios, so at a minimum it could likely detect obstacles and help a vehicle avoid a collision.

Notably, the corner images display a weak signal strength overall for both scenarios (car and no car). Compared to the front- and side-facing measurements, the corner-facing radar is

rarely normal to a large, flat surface of the vehicle, so the incident electromagnetic waves are more likely to scatter in other directions than return to the radar. In other words, the impact of specular reflections increases at corner features. Looking at the signal strength difference image in Figure 12, there is arguably a distinguishable response at low to mid elevation angles in the 0° to 5° range, possibly because a road-only scenario is less likely to send reflections back to the radar at these low angles. Although this correlation could possibly allow for vehicle detection, the response is still weak and not especially useful for imaging a vehicle, especially when compared to stronger results from the front- and side-facing measurements.

In general, the idea of moving one radar to sequentially take measurements in a 6 m square grid is not very practical for self-driving applications. This arrangement was originally chosen to simplify high volume data collection for deep learning purposes, with the expectation that the form of the radar would be improved in future research. To physically move one radar to each of these points would not be feasible to capture a moving vehicle, while constructing a grid of 100 radars to take measurements simultaneously would be prohibitively expensive and introduce coupling concerns. A more realistic implementation would be an SAR-like approach using beam steering from a fixed location on the main vehicle, possibly using a similar approach to [14], but there is ongoing debate about the reliability of such a system. Alternatively, automotive radar research exists [13] using as little as two spaced, fixed radars to generate a point cloud of the target. This approach falls short on imaging detail, but it is useful for detecting and classifying objects based on sparse data.

Future Work

Further research is needed to investigate the potential benefits of applying signal processing algorithms and deep learning models to these kinds of measured data. Higher resolution measurements which would result in a final image with more than 100 pixels were avoided because of long simulation times, but they could show more detail than is currently available. Adding additional transmitters and receivers to create an antenna array could also help improve field of view, and reducing the overall range and spacing of the radar grid points would make the setup more practical for mounting on a vehicle. Furthermore, sensor fusion of radar data with lidar or camera data will be an important avenue of research to improve the robustness of the overall sensing system and reduce false alarms by checking with multiple sensors before flagging an alert. Additionally, using vehicle-to-vehicle (V2V) communication to share sensor data between vehicles is another area worth exploring to help vehicles develop a better understanding of their surroundings.

Chapter 4

Conclusion

This research explores the feasibility of using mmWave radar to image a stationary vehicle clearly enough for visual recognition. Even with a wide spacing of radar samples, the heatmaps of phase and signal strength measurements do not identifiably represent the target vehicle. The images collected do, however, present a noticeable difference in intensity between when a car is and is not present, especially for measured signal strength. This result indicates that mmWave radar is useful for detecting a vehicle's presence, but the findings are insufficient to determine whether radar can identify that an obstacle is in fact a car.

Further research is needed to evaluate whether signal processing techniques or a higher resolution sample grid could improve these images and allow for better recognition of a vehicle. The data generated in this thesis can be used for future signal processing research on this problem. Additionally, research into shrinking the radar's sampling dimensions will be necessary to enable integration of the sensing device onto a vehicle. If future work in these areas is successful, driver assistance systems and autonomous vehicles can have access to more robust obstacle detection and collision avoidance systems that can operate in a greater range of environments.

BIBLIOGRAPHY

[1] "Road traffic injuries," *World Health Organization*, Jun. 21, 2021. [Online]. Available: https://www.who.int/news-room/fact-sheets/detail/road-traffic-injuries. [Accessed: Feb. 27, 2022].

[2] L. Huang, P. Cao, B. Tan, X. Bi, and J. Bai, "System Design and Model of a 3D 79 GHz High Resolution Ultra-Wide Band Millimeter-Wave Imaging Automotive Radar," SAE Technical Paper 2018-01-1615, 2018, doi:10.4271/2018-01-1615.

[3] U.S. Department of Transportation, *Automated Driving Systems: A Vision for Safety,* Sep. 2017. [Online]. Available: https://www.nhtsa.gov/sites/nhtsa.gov/files/documents/13069a-ads2.0_090617_v9a_tag.pdf. [Accessed: Feb. 27, 2022].

[4] "Avoiding crashes with self-driving cars," *Consumer Reports,* Feb. 2014. [Online]. Available: https://www.consumerreports.org/cro/magazine/2014/04/the-road-to-self-driving-cars/index.htm#:~:text=The%20Insurance%20Institute%20for%20Highway,for%20those%20with%20automatic%20braking. [Accessed: Feb. 27, 2022].

[5] P. Gao, H. Kaas, D. Mohr, and D. Wee, "Disruptive trends that will transform the auto industry," *McKinsey & Company,* Jan. 2016. [Online]. Available: https://www.mckinsey.com/industries/automotive-and-assembly/our-insights/disruptive-trends-that-will-transform-the-auto-industry. [Accessed: Feb. 27, 2022].

[6] D. Wakabayashi, "Self-Driving Uber Car Kills Pedestrian in Arizona, Where Robots Roam," *The New York Times,* Mar. 19, 2018. [Online]. Available: https://www.nytimes.com/2018/03/19/technology/uber-driverless-fatality.html. [Accessed: Feb. 24, 2022].

[7] “Fatalities Caused by Autonomous Vehicles,” *QA Consultants.* [Online]. Available: https://qaconsultants.com/blog/fatalities-caused-by-autonomous-vehicles/. [Accessed: Feb. 27, 2022].

[8] “SAE Levels of Driving Automation Refined for Clarity and International Audience,” *SAE International*, May 3, 2021. [Online]. Available: https://www.sae.org/blog/sae-j3016-update. [Accessed: Feb. 27, 2022].

[9] “FAQ,” *Argo AI.* [Online]. Available: https://www.argo.ai/faq/. [Accessed: Feb. 27, 2022].

[10] A. Hawkins, “Cruise is now testing fully driverless cars in San Francisco,” *The Verge*, Dec. 9, 2020. [Online]. Available: https://www.theverge.com/2020/12/9/22165597/cruise-driverless-test-san-francisco-self-driving-level-4. [Accessed: Feb. 27, 2022].

[11] M. Oitzman, “SAE clarifies autonomous driving level definitions,” *The Robot Report*, May 11, 2021. [Online]. Available: https://www.therobotreport.com/sae-clarifies-autonomous-driving-level-definitions/. [Accessed: Feb. 27, 2022].

[12] G. L. Charvat, *Small and Short-Range Radar Systems.* Boca Raton, FL: CRC Press, 2014.

[13] K. Bansal, K. Rungta, S. Zhu, and D. Bharadia, “Pointillism: Accurate 3D Bounding Box Estimation with Multi-Radars,” Proc. of the 18th Conference on Embedded Networked Sensor Systems (SenSys ’20), 2020.

[14] K. Qian, Z. He, and X. Zhang, “3D Point Cloud Generation with Millimeter-Wave Radar,” Proc. ACM Interact. Mob. Wearable Ubiquitous Technol., vol. 4, no. 4, pp. 111:1-111:23, 2020.

[15] T. Slattery and K. Finnell, “Millimeter wave (MM wave) definition,” *TechTarget.* [Online]. Available: https://www.techtarget.com/searchnetworking/definition/millimeter-wave-MM-wave. [Accessed: Feb. 27, 2022].

[16] I. H. Woodhouse, *Introduction to Microwave Remote Sensing.* Boca Raton, FL, USA: CRC Press, 2006, p. 3.

[17] “Specular vs. Diffuse Reflection,” *The Physics Classroom*. [Online]. Available: https://www.physicsclassroom.com/class/refln/Lesson-1/Specular-vs-Diffuse-Reflection. [Accessed: Mar. 30, 2022].

[18] C. Wolff, “Synthetic Aperture Radar,” *radartutorial.eu.* [Online]. Available: https://www.radartutorial.eu/20.airborne/ab07.en.html. [Accessed: Mar. 18, 2022].

[19] S. Gishkori, D. Wright, L. Daniel, M. Gashinova and B. Mulgrew, "Imaging Moving Targets for a Forward-Scanning Automotive SAR," in IEEE Transactions on Aerospace and Electronic Systems, vol. 56, no. 2, pp. 1106-1119, April 2020, doi:10.1109/TAES.2019.2925446.

[20] F. J. Abdu, Y. Zhang, M. Fu, Y. Li, and Z. Deng, “Application of Deep Learning on Millimeter-Wave Radar Signals: A Review,” in Sensors, vol. 21, Mar. 10, 2021, doi:10.3390/s21061951.

[21] *Feko Getting Started Guide.* Altair Engineering, 2020. [E-book]. Available: https://2021.help.altair.com/2021/feko/. [Accessed: Mar. 31, 2022].

[22] *WinProp Getting Started Guide.* Altair Engineering, 2021. [E-book]. Available: https://2021.help.altair.com/2021.2/winprop/. [Accessed: Mar. 31, 2022].

[23] Texas Instruments, “AWR1843AOP Single-chip 77- and 79-GHz FMCW radar sensor,” AWR1843AOP datasheet, Mar. 2021 [Revised Sept. 2021].

[24] “Ansys HFSS SBR+,” *Ansys,* 2021. [Online]. Available: https://www.ansys.com/content/dam/product/electronics/hfss/ansys-sbr-plus.pdf. [Accessed: Mar. 30, 2022].

[25] “Ansys HFSS,” *Ansys,* 2022. [Online]. Available: https://www.ansys.com/products/electronics/ansys-hfss. [Accessed: Mar. 30, 2022].

[26] “Vehicle Stopping Distance Calculator,” *Computer Support Group,* May 21, 2011. [Online]. Available: http://www.csgnetwork.com/stopdistcalc.html. [Accessed: Mar. 17, 2022].

[27] “Metal properties table,” *TIBTECH innovations,* 2018. [Online]. Available: https://www.tibtech.com/conductivite.php?lang=en_US. [Accessed: Mar. 28, 2022].

ACADEMIC VITA

Abigail E. Wagner

abigailwagner101@gmail.com

EDUCATION

Bachelor of Science in Electrical Engineering
Minor in German and Certificate in International Engineering
Schreyer Honors College, The Pennsylvania State University, University Park, PA
Graduation: May 2022

ENGINEERING EXPERIENCE

Product Development Intern, *Ford Motor Company, Dearborn, MI* May - Aug 2021

- Automated the conversion of vehicle data to CAN messages for resimulation and in-house testing of a driver assistance feature
- Developed new Python and MATLAB code for file creation scripts; wrote a batch file to activate the relevant environments, call the scripts, and copy files to the cloud
- Created an automation job in Jenkins CI/CD system to run the processes above
- Collaborated with an Agile software team in a virtual setting to meet all objectives

Engineering Intern, *Penn State Bernard M. Gordon Learning Factory, University Park, PA* Jun - Aug 2020

- Designed and programmed portions of a datalogger system and temperature ramping rig alongside a research team of engineers and entomologists
- Developed and modeled a compact rig enclosure using SolidWorks

INTERNATIONAL EXPERIENCE

"Engineers Made in Germany" Program, *Pforzheim University, Pforzheim, Germany* May - Jun 2019

- Studied topics in cyber-physical systems, robotics, automotive bus systems, sustainable mobility, lasers, and production management
- Observed large-scale automotive manufacturing systems through site visits
- Developed cultural competence and German language skill

SOFTWARE

MATLAB, Python, Arduino IDE, STK (L2 Certification), Jenkins, Multisim, LabVIEW, SolidWorks

LEADERSHIP & INVOLVEMENT

Penn State Society of Women Engineers

Director of Event Logistics, *Penn State Society of Women Engineers (SWE)* Aug 2021 - Present

- Coordinate venue, materials, and food for 80+ members at general body meetings
- Lead professional development events and assist with the Engineering Career Fair

Director of Equity Recruitment, *Penn State Society of Women Engineers (SWE)* Aug 2019 - May 2021

- Led a team of students to plan a two-day event for 100 pre-college participants
- Implemented innovative program changes based on prior feedback
- Designed an interactive virtual program to engage students during COVID-19
- Collaborated with faculty advisers to coordinate recruitment and safety efforts

SWE Stayover Chair, *Penn State Society of Women Engineers (SWE)* Aug 2018 - May 2019
Participant, *National SWE Conferences (WE19 Anaheim, WE20 New Orleans, WE21 Indianapolis)* 2019 - 2021

Penn State Women in Engineering Program

Engineering Design Lead, *Penn State Women in Engineering Program Orientation (WEPO)* Mar - Aug 2021

- Created and instructed a multi-day engineering design workshop and competition themed around the National Academy of Engineering's Grand Challenges for Engineering
- Collaborated with other leads and support program directors to plan and execute a four-day orientation program for 125+ first-year students in a reinvented virtual format
- Mentored younger leadership team members to support leadership development

Mentor, *Penn State Women in Engineering Program Orientation (WEPO)* Aug 2020 - May 2021
Envoy, *Penn State Women in Engineering Program Orientation (WEPO)* Aug 2019 - May 2020

Department of Electrical Engineering

Learning Assistant, *Penn State Electrical Engineering Academic Seminar ("WE ARe…DUINO")* Aug 2020 - Present

- Prepare and teach weekly Arduino microcontroller labs to 30 first-year students
- Troubleshoot student projects and explain electrical engineering concepts

Committee Member, *Penn State Electrical Engineering Department Head Search Committee* Oct 2021 - Mar 2022

Volunteer, *Anything is Possible for Girls in Electrical Engineering (APOGEE) Camp* Jul 2020, 2021

Additional Involvement

Member, Penn State Navigators 2019 - Present

Member, Eta Kappa Nu Electrical Engineering Honor Society (IEEE-HKN), Global and PSU 2021 - Present

Member, Institute of Electrical and Electronics Engineers (IEEE), Global and PSU 2019 - Present

HONORS & AWARDS

Electrical Engineering Student Marshal, Spring 2022 Commencement 2022

William and Wyllis Leonhard Engineering Honors Program Endowment Award 2018 - 2022

John A. Tague Scholarship in Electrical Engineering 2020 - 2022

Lockheed Martin Engineering Scholar Award 2019

Penn State President's Freshman Award 2019